

PERSISTENCE IN SAMPLED DYNAMICAL SYSTEMS FASTER

U. BAUER, H. EDELSBRUNNER, G. JABŁOŃSKI AND M. MROZEK

ABSTRACT. We call a continuous self-map that reveals itself through a discrete set of point-value pairs a *sampled dynamical system*. Capturing the available information with chain maps on Delaunay complexes, we use persistent homology to quantify the evidence of recurrent behavior, and to recover the eigenspaces of the endomorphism on homology induced by the self-map. The chain maps are constructed using discrete Morse theory for Čech and Delaunay complexes, representing the requisite discrete gradient field implicitly in order to get fast algorithms.

1. INTRODUCTION

Suppose \mathbb{M} is a compact subset of \mathbb{R}^n and $f: \mathbb{M} \rightarrow \mathbb{M}$ is a continuous self-map. We study the thus defined dynamical system in the setting in which f reveals itself through a *sample*, by which we mean a finite set $X \subseteq \mathbb{M}$, a self-map $g: X \rightarrow X$, and a real number $\rho \geq d_H(X, \mathbb{M})$ such that $\|g(x) - f(x)\| \leq \rho$ for every $x \in X$, and more generally, $\|g(x) - f(y)\| \leq \rho + \|x - y\|$ for every $x \in X$ and $y \in \mathbb{M}$ with $\|x - y\| \leq d_H(X, \mathbb{M})$, where d_H denotes the Hausdorff distance. We call ρ the *approximation constant* of the sample. Calling the triplet (X, g, ρ) a *sampled dynamical system*, we formalize a concept that appears already in [EJM15]. It is less demanding than the traditional *discrete dynamical system* in which time is discrete but space is not [KMM04]. We believe that this difference is essential to make inroads into experimental settings in which pairs $(x, f(x))$ can be observed individually while the self-map remains otherwise in the dark. The approximation constant can be used to model the experimental uncertainty, but it is also needed to accommodate a finite sample. Indeed, consider for example the map $f: [0, 1] \rightarrow [0, 1]$ defined by $f(x) = \frac{x}{2}$. Letting u be the smallest positive value in a finite set $X \subseteq [0, 1]$, its image does necessarily not belong to X : $f(u) \notin X$. We call

$$(1) \quad \lambda = \max_{x, y \in X, x \neq y} \frac{\|g(x) - g(y)\|}{\|x - y\|}$$

the *Lipschitz constant* of g . It is not necessarily close to the Lipschitz constant of f , even in the case in which the ε -neighborhoods of the points in X cover \mathbb{M} . However, Kirszbraun proved that for every $g: X \rightarrow X$ there is a continuous extension $f_0: \mathbb{M} \rightarrow \mathbb{M}$ that has the same Lipschitz constant. Specifically, this is a consequence of the more general Kirszbraun Extension Property [Kir34, WeWi75]. Let \mathbb{F} be a fixed field and let $H(\mathbb{M}; \mathbb{F})$ denote the homology of \mathbb{M} with coefficients in \mathbb{F} . Hence, $H(\mathbb{M}; \mathbb{F})$ is a vector space. Since throughout the paper we only use

This research has been supported by the DFG Collaborative Research Center SFB/TRR 109 “Discretization in Geometry and Dynamics”, by Polish MNiSzW grant No. 2621/7.PR/12/2013/2, by the Polish National Science Center under Maestro Grant No. 2014/14/A/ST1/00453 and grant No. DEC-2013/09/N/ST6/02995.

homology with coefficients in the field \mathbb{F} , in the sequel we abbreviate the notation to $H(\mathbb{M})$. The map f_0 induces a linear map $H(f_0): H(\mathbb{M}; \mathbb{F}) \rightarrow H(\mathbb{M}; \mathbb{F})$. A natural characterization of this linear map are the t -*eigenvectors*. They capture homology classes invariant under the self-map up to multiplicity t , called *eigenvalue*. All t -eigenvectors form the t -*eigenspace* of the map. Starting with a finite filtration of the domain of the map, we get t -eigenspaces at every step, connected by linear maps, and therefore a finite path in the category of vector spaces, called an *eigenspace module*. The Stability Theorem in [EJM15] implies a connection between the dynamics of g and f_0 , namely that for every eigenvalue t the interleaving distance between the eigenspace modules induced by g and by f_0 is at most ε . Furthermore, the Inference Theorem in the same paper implies that for small enough ε and any eigenvalue, the eigenspace module for g gives the correct dimension of the corresponding eigenspace of the endomorphism between the homology groups of \mathbb{M} induced by f_0 .

1.1. Prior Work and Results. We continue the program started in [EJM15], with the declared goal to embed the concept of persistent homology in the computational approach to dynamical systems. Specifically, we contribute by improving the computation of persistent cyclic dynamics. This is best explained by first sketching the essential aspects of the prior method and second describing our improvement.

The construction in [EJM15] starts with a partial simplicial map from a Čech or alternatively a Vietoris–Rips complex to itself. We have such a map for every radius $r \geq 0$, which serves as a resolution parameter. Writing K_r for the complex for radius r and fixing the eigenvalue, we get a representation of the corresponding eigenspace, E_r , by comparing the identity on K_r with the partial simplicial map induced by $g: X \rightarrow X$; see Figure 1. We get partial instead of total simplicial maps

$$\begin{array}{ccccccc}
 \dots & \hookrightarrow & K_r & \hookrightarrow & \dots & \hookrightarrow & K_s & \hookrightarrow & \dots \\
 & & \downarrow & & & & \downarrow & & \\
 \dots & \hookrightarrow & K_r & \hookrightarrow & \dots & \hookrightarrow & K_s & \hookrightarrow & \dots \\
 & & & & & & & & \\
 \dots & \longrightarrow & E_r & \longrightarrow & \dots & \longrightarrow & E_s & \longrightarrow & \dots
 \end{array}$$

Figure 1: Fixing an eigenvalue, we get a nested sequence of complexes with self-maps. The left map down is the identity, while the right map down is partial and induced by g . Comparing the two maps at every step, we get a sequence of eigenspaces with linear maps between them.

because g may be expanding. It is therefore possible to have points $x, y \in X$ for which K_r contains an edge connecting x and y but not an edge connecting $g(x)$ and $g(y)$. The lack of such images causes a loss of information. In this paper, we remedy the deficiency by using a chain map to a complex for a possibly larger radius instead of a partial simplicial map to the same complex. In other words, the edge connecting x to y can be mapped to a path of edges connecting $g(x)$ and $g(y)$, and the edges on this path may be longer than the original edge. In addition to improving the accuracy of the method, we improve the efficiency of its algorithms. In particular, we use Delaunay complexes, which in contrast to Čech and Vietoris–Rips complexes do not suffer from exponential size when the radius is large. We

can therefore afford to construct the chain map to a complex for a radius that is large enough to contain all required images. As illustrated in Figure 2, we still use Čech complexes to get the chain maps and thus the eigenspaces, but we do it in a way that avoids their explicit construction. Indeed, the bottleneck of the algorithm

$$\begin{array}{ccccccc}
 \dots & \hookrightarrow & D\check{\text{Cech}}_r(X) & \hookrightarrow & \dots & \hookrightarrow & D\check{\text{Cech}}_s(X) \hookrightarrow \dots \\
 & & \downarrow & & & & \downarrow \\
 & & \check{\text{Cech}}_{\lambda r}(X) & & & & \check{\text{Cech}}_{\lambda s}(X) \\
 & & \uparrow & & & & \uparrow \\
 \dots & \hookrightarrow & D\check{\text{Cech}}_{\lambda r}(X) & \hookrightarrow & \dots & \hookrightarrow & D\check{\text{Cech}}_{\lambda s}(X) \hookrightarrow \dots \\
 \\
 \dots & \longrightarrow & E_r & \longrightarrow & \dots & \longrightarrow & E_s \longrightarrow \dots
 \end{array}$$

Figure 2: The method sketched in Figure 1 is improved by using chain maps between Delaunay–Čech complexes, which are intersections of the Delaunay triangulation with Čech complexes. They have the same homotopy type as the corresponding Delaunay complexes and are convenient substitutes for the latter. The left map down is inclusion, while the right map down is induced by g . Comparing the two maps at every step, we get again a sequence of eigenspaces with linear maps between them.

in [EJM15] is the size of the Čech or Vietoris–Rips complex, which for large values of r is exponential in the number of points in X . This explosion in size happens independent of the dimension, n , which is in sharp contrast to Delaunay complexes, whose size is at most polynomial in the number of points, namely of degree $\lceil n/2 \rceil$. In our implementation, we target the 2-dimensional situation in which the Delaunay complexes have linear size.

Our improvement uses the Čech complex in a limited capacity, namely as an intermediate step to construct the chain maps from one Delaunay complex to another, as we now explain. First, we recall the Kirschbraun intersection property for balls established by Gromov [Gro87]: letting Q be a finite set of points in \mathbb{R}^n , and $g: Q \rightarrow \mathbb{R}^n$ an injection that satisfies $\|g(x) - g(y)\| \leq \|x - y\|$ for all $x, y \in Q$, then

$$(2) \quad \bigcap_{x \in Q} B_r(x) \neq \emptyset \implies \bigcap_{x \in Q} B_r(g(x)) \neq \emptyset,$$

in which $B_r(x)$ is the closed ball with radius r and center x . Similarly, if we weaken the condition to $\|g(x) - g(y)\| \leq \lambda \|x - y\|$, for some $\lambda > 1$, then the common intersection of the balls $B_{\lambda r}(g(x))$ is non-empty. This implies that the image of the Delaunay complex for radius r includes in the Čech complex for radius λr . Second, we exploit the collapsibility of the Čech complex for radius λr to the Delaunay complex for radius λr recently established in [BaEd17]. We describe an implementation of this collapse that avoids the explicit construction of the Čech complex and uses a modification of Welzl’s miniball algorithm [Wel91] for individual steps. The expected running time for a single step is linear in the number of points, so we have a fast algorithm provided the number of steps in the collapse is not too large. While we do not have a bound on this number, our computational experiments provide evidence that it is typically small.

The most challenging aspect of our improvement is the implementation of the collapse. Using a generalization of Forman’s discrete Morse theory [For98], the proof of its existence in [BaEd17] uses the collapse from the Čech to the Delaunay–Čech complex as an intermediate step. For a given radius, the latter complex is the intersection of the Čech complex and the Delaunay triangulation. Coincidentally, a common mistake is to think that this is the Delaunay or alpha complex for the same radius. This is not correct, but it does contain the Delaunay complex as a subcomplex, and the two have the same homotopy type; see [BaEd17]. Substituting Delaunay–Čech for Delaunay complexes thus does not affect the results of our method while slightly simplifying the computations.

1.2. Outline. Section 2 describes the background in discrete Morse theory, its application to Čech and Delaunay complexes, and its extension to persistent homology. Section 3 addresses the algorithmic aspects of our method, which include the proof of collapsibility, the generalization of the miniball algorithm, and a brief review of the software that computes the eigenspaces and their persistence. Section 4 explains the circumstances under which the dimensions of the eigenspaces computed for a discrete sample are equal to the dimensions of the eigenspaces of the self-map. Section 5 presents the results of our computational experiments, comparing them with the algorithm in [EJM15]. Section 6 concludes this paper.

2. BACKGROUND

In this section, we introduce concepts from discrete Morse Theory [For98] and apply them to Čech as well as to Delaunay complexes of finite point sets [BaEd17]. We begin with the definition of the complexes and finish by complementing the picture with the theory of persistent homology.

2.1. Geometric Complexes. Our approach to dynamical systems is based on *Čech* and *Delaunay complexes*, two common ingredients in topological data analysis. In addition, we use *selective Delaunay complexes*, which interpolate between the Čech and Delaunay complexes, and *Delaunay–Čech complexes*, which offer a convenient short-cut for our method.

Čech complexes. Let $X \subseteq \mathbb{R}^n$ be finite, $r \geq 0$, and $B_r(x)$ the closed ball of points at distance r or less from $x \in X$. The *Čech complex* of X for radius r consists of all subsets of X for which the balls of radius r have a non-empty common intersection:

$$(3) \quad \check{\text{Cech}}_r(X) = \{Q \subseteq X \mid \bigcap_{x \in Q} B_r(x) \neq \emptyset\};$$

it is isomorphic to the nerve of the balls of radius r centered at the points in X . For r smaller than half the distance between the two closest points, $\check{\text{Cech}}_r(X) = X$, and for r larger than $\sqrt{2}/2$ times the distance between the two farthest points, $\check{\text{Cech}}_r(X) = 2^X$. The size of the latter complex is exponential in the number of points, which motivates the following construction.

Delaunay triangulations. The *Voronoi domain* of a point $x \in X$ consists of all points $u \in \mathbb{R}^n$ for which x minimizes the distance from u : $\text{Vor}(x, X) = \{u \in \mathbb{R}^n \mid \|x - u\| \leq \|y - u\|, \text{ for all } y \in X\}$. The *Voronoi tessellation* of X is the set of Voronoi domains $\text{Vor}(x, X)$ with $x \in X$. Assuming general position of the points in X , any two Voronoi domains are either disjoint or they intersect in a common

$(n - 1)$ -dimensional face. The *Delaunay triangulation* of X consists of all subsets of X for which the Voronoi domains have a non-empty common intersection:

$$(4) \quad \text{Del}(X) = \{Q \subseteq X \mid \bigcap_{x \in Q} \text{Vor}(x, X) \neq \emptyset\};$$

it is isomorphic to the nerve of the Voronoi tessellation. Again assuming general position, the Delaunay triangulation is an n -dimensional simplicial complex with natural geometric realization in \mathbb{R}^n . The Upper Bound Theorem for convex polytopes, see e.g. [Zie95], implies that the number of simplices in $\text{Del}(X)$ is at most some constant times the number of points to the power $\lceil n/2 \rceil$. In $n = 2$ dimensions, this is linear in the number of points, which compares favorably to the exponentially many simplices in the Čech complex.

Delaunay–Čech complexes. To combine the small size of the Delaunay triangulation with the scale-dependence of the Čech complex, we define the *Delaunay–Čech complex* of X for radius r as the intersection of the two:

$$(5) \quad \text{D}\check{\text{Cech}}_r(X) = \check{\text{Cech}}_r(X) \cap \text{Del}(X).$$

Observe that the Delaunay triangulation effectively curbs the explosive growth of simplex numbers, but does so only if the points are in general position. We will therefore assume that the points in X are in general position, justifying the assumption with computational simulation techniques that enforce this assumption in general [EdMu90].

Delaunay complexes. There is a more direct way to select subcomplexes of the Delaunay triangulation using r as a parameter. Specifically, the *Delaunay complex* of X for radius r consists of all subsets of X for which the restriction of the Voronoi domains to the balls of radius r have a non-empty common intersection:

$$(6) \quad \text{Del}_r(X) = \{Q \subseteq X \mid \bigcap_{x \in Q} [\text{Vor}(x, X) \cap B_r(x)] \neq \emptyset\};$$

it is isomorphic to the nerve of the restricted Voronoi domains. The Delaunay complexes, also known as *alpha complexes*, are the better known relatives of the Delaunay–Čech complexes. They satisfy $\text{Del}_r(X) \subseteq \text{D}\check{\text{Cech}}_r(X)$, and it is easy to exhibit sets X and radii r for which the two complexes are different. As proved in [BaEd17], the Delaunay complex has the same homotopy type as the Delaunay–Čech complex for the same radius. This is indeed the reason we can use the latter as a substitute of the former.

Selective Delaunay complexes. We finally introduce the complexes that interpolate between the Čech and Delaunay complexes of the same radius. Their role in this paper is primarily technical: to facilitate the collapse of the Čech complex to the Delaunay or the Delaunay–Čech complex. Given a subset $A \subseteq X$, the *selective Voronoi domain* of $x \in X$ consists of all points $u \in \mathbb{R}^n$ for which x is at least as close as the points in A : $\text{Vor}(x, A) = \{u \in \mathbb{R}^n \mid \|x - u\| \leq \|a - u\|, \text{ for all } a \in A\}$. For example, $\text{Vor}(x, \emptyset) = \mathbb{R}^n$. The *selective Delaunay complex* of X and A for r consists of all subsets of X for which the restricted selective Voronoi domains have a non-empty common intersection:

$$(7) \quad \text{Del}_r(X, A) = \{Q \subseteq X \mid \bigcap_{x \in Q} [\text{Vor}(x, A) \cap B_r(x)] \neq \emptyset\};$$

it is isomorphic to the nerve of the restricted selective Voronoi domains. For $A = \emptyset$, this is the Čech complex of X for r , and for $A = X$, it is the Delaunay complex of X for r . Observe that $A \subseteq B \subseteq X$ implies $\text{Vor}(x, B) \subseteq \text{Vor}(x, A)$ for every $x \in X$. It follows that $\text{Del}_r(X, B) \subseteq \text{Del}_r(X, A)$. In words, the more points of X belong to A , the more similar to the Delaunay complex is the selective Delaunay complex.

2.2. Radius Functions. All structural properties of the geometric complexes we use are conveniently expressed in terms of their radius function. In particular, the radius functions of the selective Delaunay complexes — which include the Čech and the Delaunay complexes — satisfy the conditions of a generalized discrete Morse function. We exploit this algorithmically, to collapse a Čech complex to the Delaunay–Čech complex for the same radius. The radius function of the Delaunay–Čech complex is monotonic, which is a strictly weaker property that nevertheless suffices to construct its persistent homology, as we will explain shortly.

Smallest separating spheres. Let $X \subseteq \mathbb{R}^n$ be finite and in general position, and $A \subseteq X$. An $(n - 1)$ -dimensional sphere *separates* a subset $Q \subseteq X$ from A if

- (i) all points of Q lie inside or on the sphere,
- (ii) all points of A lie outside or on the sphere.

It is possible that a point belongs to both, Q and A , in which case it must lie on the separating sphere. Given Q and A , a separating sphere may or may not exist, but if it exists, then there is a unique *smallest separating sphere*, which we denote $S(Q, A)$. We call the selective Delaunay complex for infinite radius the *selective Delaunay triangulation* of X and A , denoted $\text{Del}(X, A) = \text{Del}_\infty(X, A)$. It consists of all simplices $Q \subseteq X$ for which there exists a sphere that separates Q from A . Its *radius function* maps every simplex to the radius of the smallest separating sphere:

$$(8) \quad \mathcal{R}_{X,A}: \text{Del}(X, A) \rightarrow \mathbb{R}$$

defined by mapping $Q \in \text{Del}(X, A)$ to the radius of $S(Q, A)$. Its sublevel sets are the selective Delaunay complexes: $\mathcal{R}_{X,A}^{-1}[0, r] = \text{Del}_r(X, A)$.

For $A = \emptyset$, the selective Delaunay complex is the Čech complex: $\text{Del}_r(X, \emptyset) = \check{\text{Cech}}_r(X)$. In this case, the smallest separating sphere of a simplex is the *smallest enclosing sphere*. This sphere exists for all $Q \subseteq X$, which implies that the Čech complex for sufficiently large radii is the simplex spanned by the vertices in X : $\Delta(X) = \check{\text{Cech}}_\infty(X)$. For $A = X$, the selective Delaunay complex is the Delaunay complex: $\text{Del}_r(X, X) = \text{Del}_r(X)$. In this case, the smallest separating sphere of a simplex is the *smallest empty circumsphere*: all points of Q lie on the sphere and none of the points of X lies inside the sphere. This sphere exists iff Q belongs to the Delaunay triangulation of X .

Generalized discrete Morse functions. In a nutshell, a function on a simplicial complex, $F: K \rightarrow \mathbb{R}$, is a generalized discrete Morse function if any contiguous sublevel sets differ by a single collapse or by the deletion of a critical simplex. We are now more precise. An *interval* of K is a subset of simplices of the form $[L, U] = \{Q \mid L \subseteq Q \subseteq U\}$, in which $L \subseteq U$ are simplices in K . A *generalized discrete vector field*, V , is a partition of K into intervals. It is *acyclic* if there is a function $F: K \rightarrow \mathbb{R}$ such that $F(P) \leq F(Q)$ whenever $P \subseteq Q$, with equality holding in this case iff P and Q belong to the same interval. Such a function F is called a *generalized discrete Morse function*, and V is its *generalized discrete*

gradient. The original framework in [For98] considers only intervals of size 1 and 2. We will use this more restrictive setting as well, and when we do we will talk about (non-generalized) *discrete Morse functions* and their (non-generalized) *discrete gradients*. Given a generalized discrete gradient, it is not difficult to turn it into a discrete gradient, namely by refining each interval of size 4 or larger into pairs.

The main reason for our interest in the above formalism are its implications on the homotopy type of complexes. To discuss this connection, we note that for $L \subseteq U$, the cardinality of $[L, U]$ is $2^{\dim U - \dim L}$. If $L = U$, the interval contains only one simplex, which for this reason is called a *critical simplex* of F . The *regular simplices* of F are contained in intervals of cardinality 2 or higher. Recall that $F(P) = F(Q)$ for all simplices P, Q that belong to a common interval of F . Suppose $[L, U]$ is an interval whose simplices maximize F . It follows that $P \in [L, U]$ and $P \subseteq Q$ implies $Q \in [L, U]$. We can therefore remove all simplices of $[L, U]$ and obtain a new, smaller simplicial complex. If $\dim U - \dim L \geq 1$, then we write $K \searrow K \setminus [L, U]$ and refer to the operation as a *collapse*. If $L = U$, then removing the single simplex from K is called a *deletion*. The important difference is that a collapse preserves the homotopy type of the complex, while a deletion changes the homotopy type. We will return to this distinction shortly.

Collapsibility. Assuming X is in general position, the radius function of the selective Delaunay triangulation, $\mathcal{R}_{X,A}: \text{Del}(X, A) \rightarrow \mathbb{R}$, is a generalized discrete Morse function for every $A \subseteq X$. Moreover, $Q \subseteq X$ is a critical simplex of $\mathcal{R}_{X,A}$ iff the smallest enclosing sphere of Q is also the smallest empty circumsphere of Q ; see [BaEd17]. But this implies that the critical simplices are independent of A . In particular the Čech radius function, $\mathcal{R}_{X,\emptyset}$, has the same critical simplices as the Delaunay radius function, $\mathcal{R}_{X,X}$, and furthermore, the radius functions agree on the critical simplices. This suggests that every Čech complex collapses to the Delaunay complex for the same radius. This is indeed true but the proof is not straightforward. For example, it is not true that we can collapse $\check{\text{Cech}}_r(X)$ to $\text{Del}_r(X)$ by removing intervals of the Čech radius function. The proof of collapsibility in [BaEd17] uses a refinement of the intervals into pairs, and it includes the Delaunay–Čech complex in the result. Specifically, for every finite set $X \subseteq \mathbb{R}^n$ of points in general position and every $r \geq 0$ we have

$$(9) \quad \check{\text{Cech}}_r(X) \searrow \text{D}\check{\text{Cech}}_r(X) \searrow \text{Del}_r(X);$$

see [BaEd17, Theorem 5.10]. More about this in Section 3, where we explain how the proof of collapsibility can be implemented without explicit construction of the Čech complex.

2.3. Persistent Homology. In its original conception, persistent homology starts with a filtration of a topological space, it applies the homology functor for coefficients in a field \mathbb{F} , and it decomposes the resulting sequence of vector spaces into indecomposable summands [ELZ02]. This decomposition is unique and has an intuitive interpretation in terms of births and deaths of homology classes. We flesh out the idea using the Delaunay–Čech complexes as an example.

Let $X \subseteq \mathbb{R}^n$ be in general position, and write $F: \text{Del}(X) \rightarrow \mathbb{R}$ for the radius function whose sublevel sets are the Delaunay–Čech complexes. Specifically, $F(Q) = \mathcal{R}_{X,\emptyset}(Q)$ for every $Q \in \text{Del}(X)$. While F is not necessarily a generalized

discrete Morse function, it is *monotonic*, by which we mean $F(P) \leq F(Q)$ whenever $P \subseteq Q \in \text{Del}(X)$. Indeed, if F were not monotonic, then it would have a sublevel set that is not a complex, but we have $F^{-1}[0, r] = \check{\text{Cech}}_r(X) \cap \text{Del}(X)$, which is necessarily a complex. The Delaunay triangulation is finite, which implies that F has only finitely many sublevel sets. To index them consecutively, we write $r_1 < r_2 < \dots < r_N$ for the values of F and $K_i = F^{-1}[0, r_i]$ for the i -th Delaunay–Čech complex of X . Applying the homology functor, we get a sequence of vector spaces:

$$(10) \quad 0 = H(K_1) \rightarrow H(K_2) \rightarrow \dots \rightarrow H(K_N),$$

in which we write $H(K_i)$ for the direct sum of the homology groups of all dimensions, and the maps $h_{i,i+1}: H(K_i) \rightarrow H(K_{i+1})$ induced by the inclusions $K_i \subseteq K_{i+1}$ are linear. By composition, we have a linear map $h_{i,j}: H(K_i) \rightarrow H(K_j)$ for every $i \leq j$, and we call this structure a *persistence module*. Such a module is *indecomposable* if all vector spaces are trivial, except for an interval of 1-dimensional vector spaces, $\mathbb{F} \rightarrow \mathbb{F} \rightarrow \dots \rightarrow \mathbb{F}$, that are connected by isomorphisms. Indeed, (10) can be written as the direct sum of indecomposable modules, and this decomposition is essentially unique. If an interval starts at position i and ends at position $j-1$, then there is a homology class α *born* at K_i that *dies entering* K_j . We represent this interval by the pair (r_i, r_j) . By convention, $r_j = \infty$ if $j-1 = N$. The *dimension* of the pair is the dimension of the homology classes in the coset, and its *persistence* is $r_j - r_i$.

By construction, the rank of $H(K_i)$ is the number of indecomposable modules whose intervals cover i . It is readily computed from the multiset of pairs, which we call the *persistence diagram* of the radius function, denoted $\text{Dgm}(F)$. More generally, we can use this diagram to compute the rank of the image of $h_{i,j}$ for $i \leq j$; see e.g. [EdHa10, page 152].

3. ALGORITHMS

The main algorithmic challenge we face in this paper is the local computation of the collapse of the Čech to the Delaunay–Čech complex. Specifically, we trace edges through the collapse, using their images to construct the chain maps, which are instrumental in our analysis. We explain the algorithm in three stages: first sketching the relevant steps of the proof of existence, second describing how we compute minimum separating spheres, and third explaining the discrete flow that constructs the chain map. Once we arrive at the eigenspaces, we compute their persistent homology with the software implementing the algorithms in [EJM15]. We end this section with a description of the steps necessary to compute persistent homology of the eigenspaces.

3.1. Proof of Collapsibility. The complete proof of collapsibility can be found in [BaEd17]. Its main technical ingredients are Lemmas 5.5 to 5.8 stated and proved in that paper, and only the latter two are relevant to our algorithm. Indeed, Lemmas 5.5 and 5.6 concern themselves with the collapse from the Delaunay–Čech to the Delaunay complex, which we ignore. Lemmas 5.7 and 5.8 concern themselves with the collapse from the Čech to the Delaunay–Čech complex, which we use. We restate their combined claims for the special case in our interest.

Proposition 1. *Letting $Q \subseteq X$, we write $Q - x = Q \setminus \{x\}$ and $Q + x = Q \cup \{x\}$, noting that one of them is equal to Q . There is a map $\psi: \Delta(X) \setminus \text{Del}(X) \rightarrow X$ such that for every $Q \in \Delta(X) \setminus \text{Del}(X)$ there exists a vertex $x \in X$ with*

- (i) $x = \psi(Q - x) = \psi(Q + x)$,
- (ii) $S(Q - x, \emptyset) = S(Q + x, \emptyset)$,
- (iii) both $Q - x$ and $Q + x$ do not belong to $\text{Del}(X)$.

The map ψ implies a partition of $\Delta(X) \setminus \text{Del}(X)$ into pairs of the form $(Q - x, Q + x)$. Because of (ii), a subset of these pairs partitions $\check{\text{Cech}}_r(X) \setminus \text{Del}(X)$, and removing these pairs in sequence collapses $\check{\text{Cech}}_r(X)$ to $\check{\text{Cech}}_r(X) \cap \text{Del}(X) = \text{D}\check{\text{Cech}}_r(X)$. It remains to discuss how ψ is constructed. As explained in the proof of Lemma 5.8 in [BaEd17], we use an arbitrary but fixed ordering x_1, x_2, \dots, x_N of the points in X . For each simplex, we iterate through the points, excluding them from inside the separating sphere until we reach a situation in which no such sphere exists any more. To formalize this process, let $Q \in \Delta(X) \setminus \text{Del}(X)$, and let $A_j \subseteq X$ contain all points x_i for which $i \leq j$ or x_i lies already on or outside $S(Q, \emptyset)$. There is a unique index $j < N$ such that $A = A_j$ and $x = x_{j+1}$ satisfy $Q \in \text{Del}(X, A) \setminus \text{Del}(X, A + x)$, and we use this choice of vertex to define $\psi(Q) = x$. To compute $\psi(Q)$, it thus suffices to work through the sequence A_0, A_1, \dots, A_{N-1} and find the first set, $A = A_j$, for which there is no sphere that separates Q from $A + x = A_{j+1}$. We discuss how this is done next.

3.2. Separating Spheres. At the core of the discrete flow algorithm is the capability to compute the smallest separating sphere of sets $Q, A \subseteq X$, or deciding that it does not exist. We pattern the algorithm after the randomized algorithm for the smallest enclosing sphere described in [Wel91], which we recall first.

Welzl's randomized miniball algorithm. The smallest enclosing sphere of a set $Q \subseteq \mathbb{R}^n$ is determined by at most $n + 1$ of the points. In other words, there is a subset $R \subseteq Q$ of at most $n + 1$ points such that the smallest enclosing sphere of R is also the smallest enclosing sphere of Q . The algorithm below makes essential use of this observation. It partitions Q into two disjoint subsets: R containing the points we know lie on the smallest enclosing sphere, and $P = Q \setminus R$. Initially, $R = \emptyset$ and $P = Q$. In a general step, the algorithm removes a random point from P and tests whether it lies on or inside the recursively computed smallest enclosing sphere of the remaining points. If yes, the point is discarded, and if no, the point is added to R .

```

1  sphere ENCLOSE( $P, R$ ):
2    if  $P = \emptyset$  then let  $S$  be the smallest circumsphere of  $R$ 
3    else choose a random point  $p \in P$ ;
4          $S = \text{ENCLOSE}(P \setminus \{p\}, R)$ ;
5         if  $p$  outside  $S$  then  $S = \text{ENCLOSE}(P \setminus \{p\}, R \cup \{p\})$ ;
6  return  $S$ .
```

Since the algorithm makes random choices, its running time is a random variable. Remarkably, the expected running time is linear in the number of points in Q , and the reason is the high probability that the randomly chosen point, p , lies inside the recursively computed smallest enclosing sphere and can therefore be discarded.

Generalization to smallest separating spheres. Rather than enclosing spheres, we need separating spheres to compute the collapse. Here we get an additional case, when the sphere does not exist, which we indicate by returning NULL. As before, we work with two sets of points: R containing the points we know lie on the smallest separating sphere, and P containing the rest. Initially, $R = Q \cap A$ and $P = (Q \cup A) \setminus R$. Each point has enough memory to remember whether it belongs to Q and thus needs to lie on or inside the sphere, or to A and thus needs to lie on our outside the sphere. We say the point *contradicts* S if it lies on the wrong side.

```

1  sphere SEPARATE( $P, R$ ):
2    if card  $R > n + 1$  then return NULL;
3    if  $P = \emptyset$  then let  $S$  be the smallest circumsphere of  $R$ 
4        else choose a random point  $p \in P$ ;
5             $S = \text{SEPARATE}(P \setminus \{p\}, R)$ ;
6            if  $p$  contradicts  $S$  then  $S = \text{SEPARATE}(P \setminus \{p\}, R \cup \{p\})$ ;
7  return  $S$ .
```

Since the smallest separating sphere is again determined by at most $n + 1$ of the points, the expected running time of the algorithm is linear in the number of points, as before.

Iterative version with move-to-front heuristic. Because finding separating spheres is at the core of our algorithm, we are motivated to improve its running time, even if it is only by a constant factor. Following the advice in [Gar99], we turn the tail-recursion into an iteration and combine this with a move-to-front heuristic. Indeed, if a point contradicts the current sphere, it is likely that it does the same to a later computed sphere. The earlier the point is tested, the faster this new sphere can be rejected. Storing the points in a linear list, early testing of this point can be enforced by moving it to the front of the list. Write \mathcal{L} for the list, which contains all points of $Q \cup A$, and write $\mathcal{L}(i)$ for the point stored at the i -th location. As before, each point remembers whether it belongs to Q , to A , or to both. In addition, we mark the points we know lie on the smallest separating sphere as members of R , initializing this set to $R = Q \cap A$. Furthermore, we initialize $N = \text{card}(Q \cup A)$.

```

1  sphere MOVETOFRONT( $\mathcal{L}, N, R$ ):
2    if card  $R > n + 1$  then return NULL;
3    let  $S$  be smallest circumsphere of  $R$ ;
4    for  $i = 1$  to  $N$  do
5        if  $p = \mathcal{L}(i)$  contradicts  $S$  then  $S = \text{MOVETOFRONT}(\mathcal{L}, i - 1, R \cup \{p\})$ ;
6            if  $S = \text{NULL}$  then return NULL;
7            move  $p$  to front of  $\mathcal{L}$ ;
8  return  $S$ .
```

Section 5 will present experimental evidence that the move-to-front heuristic accelerates the computations.

3.3. Constructing the Chain Map. We now have the necessary prerequisites to construct the chain map. Specifically, given a 1-cycle in $\text{D}\check{\text{Cech}}_r(X)$, we are interested in computing its image, which is a 1-cycle in $\text{D}\check{\text{Cech}}_s(X)$, with $r \leq s \leq \lambda r$. We begin with the underlying concepts from discrete Morse theory.

Discrete flow. We follow the notation in [For98] in which the discrete flow is formulated as a map on chains. Let K be a simplicial complex and $F: K \rightarrow \mathbb{R}$ a (non-generalized) discrete Morse function with (non-generalized) discrete gradient ∇F . Recall that this means that every interval in ∇F is either a pair or a singleton. In the most relevant example, $K = \check{\text{Cech}}_r(X)$ and ∇F contains all pairs defined by the map ψ in the proof of collapsibility. These pairs partition $\check{\text{Cech}}_r(X) \setminus D\check{\text{Cech}}_r(X)$, and not the entire Čech complex, but this is easily remedied by partitioning $D\check{\text{Cech}}_r(X)$ into singletons and adding them to ∇F . It is convenient to write the discrete gradient as a function:

$$(11) \quad \nabla F(P) = \begin{cases} -\langle P, \partial Q \rangle Q & \text{if } (P, Q) \in V, \\ 0 & \text{otherwise,} \end{cases}$$

where ∂ stands for the boundary operator and $\langle \cdot, \cdot \rangle$ denotes the inner product, defined on the chain group $\mathcal{C}(K)$ by declaring the simplices of K to be an orthonormal basis. It maps every oriented p -simplex to 0 or to a $(p+1)$ -simplex. We linearly extend the function to $\nabla F: \mathcal{C}(K) \rightarrow \mathcal{C}(K)$, which maps every p -chain to a possibly trivial $(p+1)$ -chain. Recall that $\partial: \mathcal{C}(K) \rightarrow \mathcal{C}(K)$ is another linear map that maps every p -chain to a possibly trivial $(p-1)$ -chain. We use both to introduce $\Phi: \mathcal{C}(K) \rightarrow \mathcal{C}(K)$ defined by mapping a p -chain c to

$$(12) \quad \Phi(c) = c + \partial(\nabla F(c)) + \nabla F(\partial(c)),$$

which is a possibly trivial p -chain. We call Φ the *discrete flow* induced by ∇F . Importantly, it commutes with the boundary map, which makes it a chain map; see [For98, Theorem 6.4]. Moreover, the iteration of Φ stabilizes in the sense that $\Phi^M = \Phi^N$ for M, N large enough [For98, Theorem 7.2]. We denote this sufficiently high iterate by Φ^* .

Proposition 2. *Let K be a simplicial complex and $\Phi: \mathcal{C}(K) \rightarrow \mathcal{C}(K)$ the discrete flow induced by a discrete gradient on K . Then $\partial\Phi = \Phi\partial$.*

There is a single-line proof, which we give for completeness. Using shorthand notation and $\partial^2 = 0$, we have

$$(13) \quad \Phi\partial = (1 + \partial\nabla F + \nabla F\partial)\partial = \partial + \partial\nabla F\partial = \partial(1 + \nabla F\partial + \partial\nabla F) = \partial\Phi.$$

In this paper, we apply the discrete flow exclusively to 1-cycles. In other words, $c \in \mathcal{C}(K)$ is 1-dimensional with $\partial c = 0$. Hence, $\nabla F(c)$ is either trivial or a 2-chain, and $\Phi(c) = c + \partial(\nabla F(c))$. While this simplification is convenient, it is not necessary for our technical discussion, which applies generally to chains of any dimension.

Computing the discrete flow. The implementation of the discrete flow is primarily a translation of mathematical into computational notation. To compute the boundary of a chain, we add the boundaries of the individual simplices keeping track of simplices' coefficients in the chain:

```

1  chain BD(c):
2    b = 0; forall summands  $\alpha Q$  of  $c$  do forall  $x \in Q$  do  $b = b + \alpha Q_x$ ;
3    return b,
```

where Q_x denotes the oriented face obtained by removing the vertex x from Q . Note that $Q_x = \langle Q - x, \partial Q \rangle (Q - x)$ can be computed efficiently without using the inner product. Similarly, the gradient of a chain is computed by adding the

gradients of its simplices. For convenience, we overload the function `GRAD` so its argument can be a chain or a simplex. In the former case, we have

```

1  chain GRAD(c):
2    d = 0; forall summands  $\alpha Q$  of c do d = d +  $\alpha$ GRAD(Q);
3    return d.
```

If applied to a single simplex, the gradient function follows the proof of collapsibility. Given a fixed ordering of the points in X and a simplex Q , we let $A_j \subseteq X$ consist of the first j points in the ordering together with all points on or outside the smallest enclosing sphere of Q . The function searches for the smallest index, j , such that there is no separating sphere for Q and A_{j+1} .

```

1  simplex GRAD(Q):
2    S = ENCLOSE(Q);
3    let  $A_0 \subseteq X$  contain all points on or outside S;  $A = A_0$ ;  $j = 0$ ;
4    while  $j < N$  and SEPARATE(Q, A)  $\neq$  NULL do  $j = j + 1$ ;  $A = A \cup \{x_j\}$ ;
5    if  $j < N$  then return  $Q + x_{j+1}$ ;
6    return NULL.
```

Instead of `ENCLOSE` and `SEPARATE` we may of course call `MOVETOFRONT`, which takes different input parameters but yields the same results. Finally, we combine the boundary and gradient to compute the discrete flow:

```

1  chain PHI(c):
2    d = 0;
3    forall summands  $\alpha Q$  of c do d = d +  $\alpha Q$  + BD(GRAD( $\alpha Q$ )) + GRAD(BD( $\alpha Q$ ));
4    return d.
```

In our application, the sum of boundaries is necessarily trivial, so we can simplify the computation by dropping `Grad(BD(Q))`, thus working with what Forman calls the reduced flow [For98]. We emphasize that we usually iterate `PHI` until it stabilizes; see Proposition 2 and the definition of Φ^* right before.

3.4. Eigenspaces and Their Persistence. We use the chain maps connecting the Delaunay–Čech complexes to extract eigenspaces, maps between the eigenspaces, and their persistence. We explain this in three steps: first establishing the filtration, second constructing the eigenspaces, and third computing the maps between them and their persistence.

Filtration. Given a finite set $X \subseteq \mathbb{R}^n$, we use software from the CGAL library [CGAL16] to construct the filtration of Delaunay–Čech complexes. While this functionality is currently not offered by CGAL, it is easy to adapt this software for this purpose. In particular, we first compute the Delaunay triangulation, $\text{Del}(X)$, and second determine the smallest enclosing sphere for each of its simplices, effectively constructing the Čech radius function restricted to the Delaunay triangulation, $F: \text{Del}(X) \rightarrow \mathbb{R}$. Recall that the sublevel sets of F are the Delaunay–Čech complexes of X : $\text{DČech}_r(X) = F^{-1}[0, r]$ for every $r \geq 0$.

Writing $r_1 < r_2 < \dots < r_N$ for the values of F , we thus get a nested sequence of complexes $K_i = F^{-1}[0, r_i]$ for $1 \leq i \leq N$. Using our own implementation of the persistence algorithm, we compute the persistence diagram of this filtration, which is a multiset of intervals of the form $[r_i, r_j]$. For each interval, there is a unique homology class born at K_i that maps to 0 when it dies entering K_j . The thus

obtained homology classes give a basis for the homology groups of every complex in the filtration.

Eigenspaces. To compute the eigenspace for K_i , we consider two maps between homology groups, $\iota_i, \kappa_i: H(K_i) \rightarrow H(K_j)$, in which $i \leq j$, ι_i is induced by the inclusion $K_i \subseteq K_j$, and κ_i is induced by the chain map composed of g followed by Φ^* . The index $j \geq i$ is chosen as small as possible such that all loops in K_i have images in K_j , as we explain shortly. It is guaranteed that the corresponding radius satisfies $r_j \leq \lambda r_i$, in which λ is the Lipschitz constant of g .

We are now more specific about the construction of the two maps, ι_i and κ_i , which we represent in matrix form. Writing ℓ for the rank of the first homology group of K_i , we have ℓ generators, and we choose a representative cycle for each, referring to the resulting ℓ cycles as the *loops* of K_i . Each loop, c , is mapped to a 1-cycle c' in K_j using the discrete flow, Φ^* . Expressing the homology class of c' as a sum of the generators of $H(K_j)$ — as computed by the persistence algorithm — we get a column of the matrix of κ_i . Repeating these computations for all loops of K_i , we get κ_i . We compute the matrix of ι_i in a similar fashion.

Fixing an eigenvalue, t , we construct the corresponding eigenspace E_i^t , which is a sub-quotient of $H(K_i)$, by taking $\ker(\kappa_i - t\iota_i)$ modulo $\ker \kappa_i \cap \ker \iota_i$; see also [EJM15]. In words, E_i^t is generated by the loops in K_i whose images under κ_i are homologous to t times their images under the inclusion, ι_i . Note that we use a slight modification of the classic eigenvalue problem in which the image and the range are identical. This is not the case for κ_i , so we compare it to ι_i to get the eigenspace.

Maps and persistence. The maps between the eigenspaces are obtained as restrictions of the linear maps $h_{i,i+1}: H(K_i) \rightarrow H(K_{i+1})$, which are induced by inclusion. For a fixed $t \in \mathbb{F}$, we have a sequence of eigenspaces, E_i^t , and for each $1 \leq i < N$, we construct $\gamma_i: E_i^t \rightarrow E_{i+1}^t$ by mapping every class $\alpha \in E_i^t$ to $\gamma_i(\alpha) = h_{i,i+1}(\alpha)$. This results in

$$(14) \quad 0 \rightarrow E_1^t \rightarrow E_2^t \rightarrow \dots \rightarrow E_N^t,$$

and by composing the connecting linear maps, we get a persistence module. While it is more general than the persistence module described in Section 2.3, the unique decomposition into indecomposable modules (intervals) is guaranteed [EJM15, Basis Lemma]. We can therefore compute the persistence diagram, which we refer to as the *eigenspace diagram* of g for eigenvalue t , denoted $\mathbf{Egm}(g, t)$.

4. INFERENCE

We now describe how the sample g and the persistence module of eigenspaces in (14) can be used to infer the homology eigenspaces of the continuous self-map f . Recall that $B_\delta(x)$ is the closed ball of radius δ centered at $x \in \mathbb{R}^n$. For a compact subset $K \subseteq \mathbb{R}^n$, we write $K_\delta = \bigcup_{x \in K} B_\delta(x)$ for the closed δ -neighborhood of K . By the Kirszbraun Extension Property [Kir34, WeWi75], f extends to a map $f_\delta: \mathbb{M}_\delta \rightarrow \mathbb{M}_\delta$ with the same Lipschitz constant for any $\delta > 0$. Choosing $\delta > 0$ so that $\mathbb{M} \subseteq X_\delta$, and choosing $\rho \geq \delta$ such that $f(B_\delta(x)) \subseteq B_{\rho+\delta}(g(x))$ for all $x \in X$; note that this is true if we choose $\delta = d_H(X, \mathbb{M})$ and ρ as the approximation constant of g . we consider the extensions $f_\delta: \mathbb{M}_\delta \rightarrow \mathbb{M}_\delta$ and $f_{\rho+\delta}: \mathbb{M}_{\rho+\delta} \rightarrow \mathbb{M}_{\rho+\delta}$. Assume that the map $H(\mathbb{M}) \rightarrow H(\mathbb{M}_\delta)$ induced by inclusion is an isomorphism, while

the map $H(\mathbb{M}_\delta) \rightarrow H(\mathbb{M}_{\rho+\delta})$ induced by inclusion is an monomorphism. If the above assumptions are satisfied, we call (X, g, ρ) a *well-sampled dynamical system*. We now have the following commutative diagram, in which all maps are induced by inclusions unless specified otherwise:

$$(15) \quad \begin{array}{ccccc} & & H(X_\delta) & \xrightarrow{\iota} & H(X_{\rho+\delta}) \\ & \nearrow & \searrow a & \nearrow b & \searrow \\ H(\mathbb{M}) & \hookrightarrow & H(\mathbb{M}_\delta) & \hookrightarrow & H(\mathbb{M}_{\rho+\delta}) \\ \downarrow f & & \downarrow f_\delta & & \downarrow f_{\rho+\delta} \\ H(\mathbb{M}) & \hookrightarrow & H(\mathbb{M}_\delta) & \hookrightarrow & H(\mathbb{M}_{\rho+\delta}) \\ & \searrow & \nearrow a & \searrow b & \nearrow \\ & & H(X_\delta) & \xrightarrow{\iota} & H(X_{\rho+\delta}) \end{array}$$

Let $a: H(X_\delta) \rightarrow H(\mathbb{M}_\delta)$, $b: H(\mathbb{M}_\delta) \rightarrow H(X_{\rho+\delta})$, and $\iota: H(X_\delta) \rightarrow H(X_{\rho+\delta})$ be induced by inclusion, and define $\phi = b \circ f_\delta \circ a: H(X_\delta) \rightarrow H(X_{\rho+\delta})$. Furthermore, let

$$(16) \quad E^t(\phi, \iota) = \ker(\phi - t\iota) / (\ker \phi \cap \ker \iota)$$

be the eigenspace of the pair ϕ and ι , and let $E^t(f)$ be the eigenspace of f , both for the eigenvalue t .

Lemma 3. *With the above assumptions, $E^t(\phi, \iota) \cong E^t(f)$.*

Proof. Since $\phi = b \circ f_\delta \circ a$ and $\iota = b \circ a$, with b injective, we have $\ker a \subseteq \ker \phi$ and $\ker \iota = \ker a$, and therefore $\ker \phi \cap \ker \iota = \ker a$. This implies

$$(17) \quad E^t(\phi, \iota) = \ker(\phi - t\iota) / (\ker \phi \cap \ker \iota)$$

$$(18) \quad = \ker(b \circ f_\delta \circ a - tb \circ a) / \ker a$$

$$(19) \quad \cong \ker(b \circ f_\delta - tb).$$

Moreover, since b is a monomorphism, we have

$$(20) \quad \ker(b \circ f_\delta - tb) \cong E^t(f_\delta),$$

concluding the proof since $H(\mathbb{M}) \cong H(\mathbb{M}_\delta)$ and thus $E^t(f_\delta) \cong E^t(f)$. \square

To apply this lemma to eigenspaces constructed from Čech complexes, we need the following version of the famous Nerve Theorem, which is compatible with persistence. We recall that a cover of a topological space is *good* if the common intersection of any sub-cover is either empty or contractible. We denote the *nerve* of a cover \mathcal{U} by $N(\mathcal{U})$.

Proposition 4 (Functorial Nerve Theorem [ChOu08]). *Let $\mathbb{X} \subseteq \mathbb{Y}$, and let $\mathcal{U} = (U_i)_{i \in I}, \mathcal{V} = (V_j)_{j \in J}$ be good covers of \mathbb{X} and \mathbb{Y} , respectively. Let $g: I \rightarrow J$ be such that $f(U_i) \subseteq V_{g(i)}$ for all $i \in I$. Then the simplicial map γ induced by g is naturally homotopy equivalent to the inclusion $\mathbb{X} \hookrightarrow \mathbb{Y}$, i.e., the following diagram in which*

the vertical arrows are homotopy equivalences commutes:

$$(21) \quad \begin{array}{ccc} \mathbb{X} & \hookrightarrow & \mathbb{Y} \\ \simeq \downarrow & & \downarrow \simeq \\ N(\mathcal{U}) & \xrightarrow{\gamma} & N(\mathcal{V}) \end{array}$$

Now consider the self-map $g: X \rightarrow X$. Recall that $f(B_\delta(x)) \subseteq B_{\rho+\delta}(g(x))$ for all $x \in X$. Then g defines a simplicial map $\check{\text{Cech}}_\delta(X) \rightarrow \check{\text{Cech}}_{\rho+\delta}(X)$, which in turn induces a map $\gamma: H(\check{\text{Cech}}_\delta(X)) \rightarrow H(\check{\text{Cech}}_{\rho+\delta}(X))$ in homology. Letting $j: H(\check{\text{Cech}}_\delta(X)) \hookrightarrow H(\check{\text{Cech}}_{\rho+\delta}(X))$ be the inclusion homomorphism, the following diagrams commute by the Functorial Nerve Theorem:

$$(22) \quad \begin{array}{ccc} H(X_\delta) & \xrightarrow{\phi} & H(X_{\rho+\delta}) \\ \cong \downarrow & & \downarrow \cong \\ H(\check{\text{Cech}}_\delta(X)) & \xrightarrow{\gamma} & H(\check{\text{Cech}}_{\rho+\delta}(X)) \end{array} \quad \begin{array}{ccc} H(X_\delta) & \xrightarrow{\iota} & H(X_{\rho+\delta}) \\ \cong \downarrow & & \downarrow \cong \\ H(\check{\text{Cech}}_\delta(X)) & \xrightarrow{j} & H(\check{\text{Cech}}_{\rho+\delta}(X)) \end{array}$$

Theorem 5. *With the above assumptions, $E^t(f) \cong E^t(\phi, \iota) \cong E^t(\gamma, j)$.*

Proof. The maps at the top satisfy the assumptions of the diagram (15), so Lemma 3 applies and proves the first isomorphism. The commutativity of the diagrams (22) implies the second isomorphism. \square

To relate the result back to our algorithm, we note that δ is constrained by the sample, X , and the sample is constrained by the assumption that the map $H(\mathbb{M}) \rightarrow H(\mathbb{M}_\delta)$ induced by inclusion be an isomorphism. On the other hand, $\rho \geq \delta$ is constrained by the assumption that the induced map $H(\mathbb{M}_\delta) \rightarrow H(\mathbb{M}_{\rho+\delta})$ is a monomorphism, and the image under f of a ball with radius δ centered at $x \in X$ is contained in the ball of radius $\rho + \delta$ centered at $g(x)$. Our algorithm finds the smallest value such that it can construct the required maps on the level of Čech complexes. The dimension of $E^t(f)$ can now be read off the eigenspace diagram $\text{Egm}(g, t)$:

Theorem 6. *Let (X, g, ρ) be a well-sampled dynamical system for the self-map \mathbb{M} , and let $\delta = d_H(X, \mathbb{M})$. Choose i, j such that $\delta \in [r_i, r_{i+1})$ and $\rho + \delta \in [r_j, r_{j+1})$. Then*

$$E^t(f) \cong h_{i,j}(E_i^t).$$

Proof. From Theorem 5 we get $E^t(f) \cong E^t(\gamma, j)$, and the isomorphism $E^t(\gamma, j) \cong h_{i,j}(E_i^t)$ follows from the collapsibility result (9) and the construction of the eigenspace module (14) described in Section 3. \square

Note that $\dim h_{i,j}(E_i^t)$ is the number of intervals in $\text{Egm}(g, t)$ containing $[i, j)$ as a subinterval.

5. COMPUTATIONAL EXPERIMENTS

In this section, we analyze the performance of our algorithm experimentally and compare the results with those reported in [EJM15]. For ease of reference, we call the algorithm in [EJM15] the *Vietoris-Rips* or *VR-method* and the algorithm in this paper the *Delaunay-Čech* or *DČ-method*. We begin with the introduction of

the case-studies — self-maps on a circle and a torus — and end with statistics collected during our experiments.

5.1. Expanding Circle Map. The first case-study is an expanding map from the circle to itself. To add noise, we extend it to a self-map on the plane, $f: \mathbb{C} \rightarrow \mathbb{C}$ defined by $f(z) = z^2$. While traversing the circle once, the image under f travels around the circle twice. To generate the data, we randomly chose N points on the unit circle, and letting z_i be the i -th such point, we pick a point x_i from an isotropic Gaussian distribution with center z_i and width $\sigma = 0.1$. Write X for the set of all points x_i , and let the image of x_i be the point $g(x_i) \in X$ that is closest to x_i^2 . As explained earlier, we construct the filtration of Delaunay–Čech complexes of X and compute eigenspace diagrams for all eigenvalues in a sufficiently large finite field. Our choice is $\mathbb{F} = \mathbb{Z}_{1009}$.

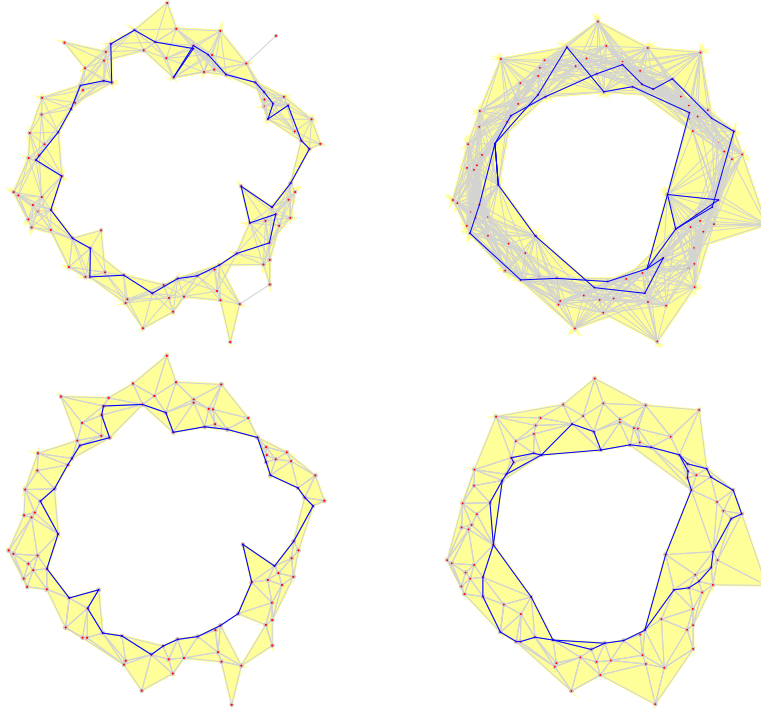


Figure 3: *Top row:* a loop representing the eigenvector for eigenvalue $t = 2$ in the VR-method on the *left* and its image on the *right*. *Bottom row:* the corresponding loop for $t = 2$ in the DČ-method on the *left* and its image on the *right*. While the VR-method uses the same radius for the original loop and its image, we show the Vietoris–Rips complexes for different radii, namely about the same as for the Delaunay–Čech complexes below to illustrate the dependence of the size difference on the radius parameter.

Drawing $N = 100$ points, we compare the DČ-method of this paper with the VR-method in [EJM15]. For eigenvalue $t = 2$, both methods give a non-empty eigenspace diagram consisting of a single point. Figure 3 illustrates the results by showing the generating loop on the left and its image on the right, first for the VR-method and second for the DČ-method. Observe that the Vietoris–Rips complexes

have many more simplices than the Delaunay–Čech complexes for the same radius, in particular for larger radii. The difference illustrates the improvement in running time we get using the DČ-method.

5.2. Torus Maps. The second case-study consists of three self-maps on the torus, which we construct as a quotient of the Cartesian plane; see Figure 4. For $i = 1, 2, 3$, the map $f_i: [0, 1)^2 \rightarrow [0, 1)^2$ sends a point $x = (x_1, x_2)^T$ to $f_i(x) = A_i x$, in which

$$A_1 = \begin{bmatrix} 2 & 0 \\ 0 & 2 \end{bmatrix}, \quad A_2 = \begin{bmatrix} 0 & 1 \\ 1 & 0 \end{bmatrix}, \quad A_3 = \begin{bmatrix} 1 & 1 \\ 0 & 1 \end{bmatrix}.$$

The 1-dimensional homology group of the torus has only two generating loops. Letting one wrap around the torus in meridian direction and the other in longitudinal direction, we see that f_1 doubles both generators, f_2 exchanges the generators, and f_3 adds them but also preserves the first generator. Correspondingly, f_1 has two

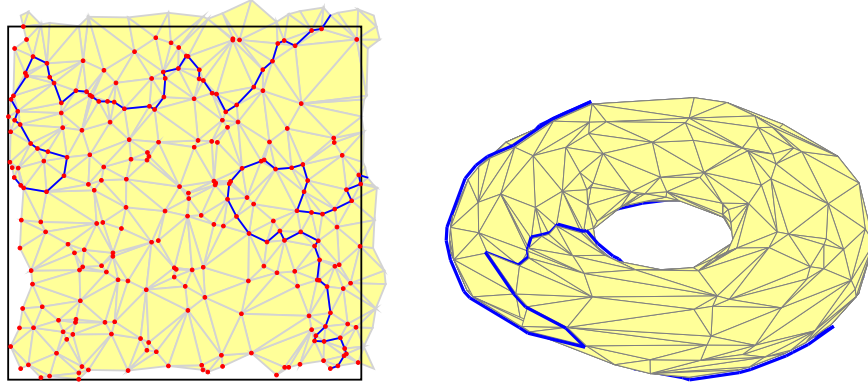


Figure 4: The periodic Delaunay triangulation on the *left* and its embedding in \mathbb{R}^3 on the *right*. The blue loop wraps around the torus once in meridian and once in longitudinal direction. It represents an eigenvector of f_1 for eigenvalue $t = 2$. Its image wraps around the torus twice in meridian and twice in longitudinal direction (not shown).

eigenvectors for the eigenvalue $t = 2$, f_2 has two distinct eigenvalues $t = 1$ and $t = -1$, and f_3 has only one eigenvector for $t = 1$. The input data for our algorithm, X , consists of 100 points uniformly chosen in $[0, 1)^2$. To define the image of a point $x \in X$, we compute the point $A_i x$ and let the image be the nearest point $g_i(x) \in X$. The eigenspace diagrams of f_1, f_2, f_3 for selected eigenvalues are shown in the last three panels of Figure 5.

5.3. Accuracy. To study how accurate the two methods are, we look at *false positives* and *false negatives*, and the persistence of the recurrent features of the underlying smooth maps.

Circle map. Repeating the circle map experiment with $N = 100$ points ten times, we show the superimposed twenty eigenspace diagrams (ten each for the two methods) in the upper left panel of Figure 5. Points of the VR-method are marked blue while points of the DČ-method are marked red. The eigenvector for $t = 2$ is detected each time. However, the DČ-method detects the recurrence consistently earlier than the VR-method, with smaller birth and death values but also with

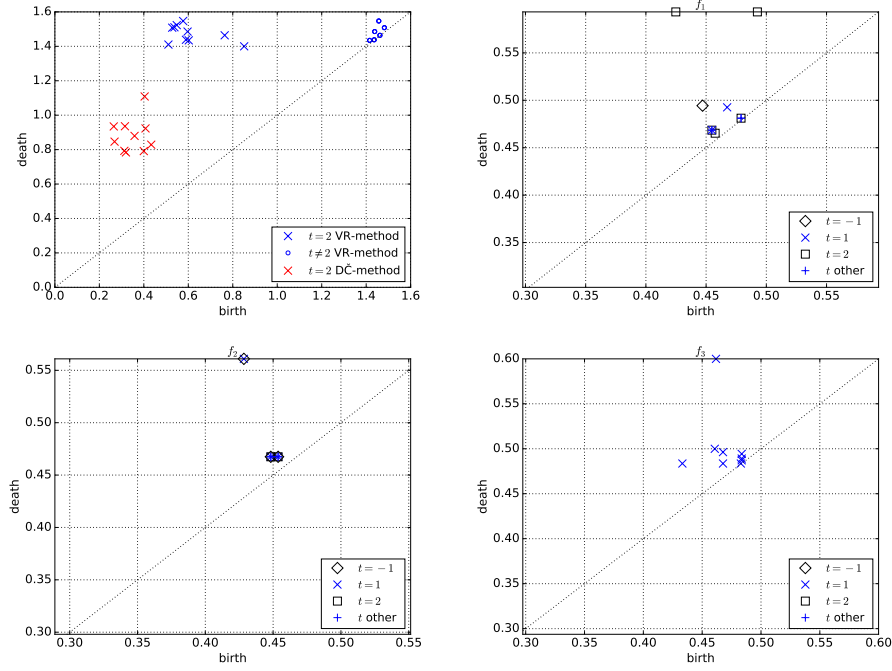


Figure 5: *Top left panel:* the superimposed eigenspace diagrams of the expanding circle map for ten randomly chosen sets of 100 points each. The intervals are plotted as points whose coordinates are the birth and death values of the corresponding homology classes. Points for the VR-method are blue and points of the DČ-method are red. The only points with non-negligible persistence belong to eigenvalue $t = 2$, and we get exactly one such point for each eigenspace diagram. *Top right panel:* the eigenspace diagrams of f_1 for a few eigenvalues. The most persistent classes are represented by points at the upper edge of the panel, indicating that their intervals last all the way to the last complex in the filtration. Here we see two such points, which correspond to the intrinsic 1-dimensional homology of the torus. *Bottom left panel:* the eigenspace diagrams of f_2 for a few eigenvalues. There are two intervals that exists during most of the filtration, one for eigenvalue $t = 1$ and the other for eigenvalue $t = -1$. They have the same birth and death and are therefore visible as two identical points on the upper edge of the panel. *Bottom right panel:* the eigenspace diagrams of f_3 for a few eigenvalues. There is only one significant eigenvector for $t = 1$.

smaller average persistence. The shift of the birth values is easy to rationalize: a loop arises for the same radius in both filtrations, but remains without image in the VR-method until the radius is large enough to capture the image of every edge in the loop. The shift of the death value is more difficult to explain and perhaps related to the fact that the DČ-method maps a loop in one complex, K_r , to a later complex, K_s with $r \leq s \leq \lambda r$ in the filtration of Delaunay–Čech complexes. Monitoring r and s in 100 runs for a range of number of points, we show the average Lipschitz constant and the average ratio $\frac{s}{r}$ in Table 1. There are no false negatives in this experiment, but we see a small number of false positives reported by the VR-method (the points in the upper right corner of the first panel in Figure 5, all for eigenvalues $t \neq 2$). This indicates that the VR-method is more susceptible to noise

	$N = 100$	200	300	400	500
average λ	1.99	2.00	2.05	2.03	2.04
average s/r	1.13	1.14	1.12	1.14	1.16
average λ	2.65	3.54	3.98	4.22	5.42
average s/r	1.33	1.57	1.71	1.64	1.91

Table 1: The average Lipschitz constant, λ , and the average shift, $\frac{s}{r}$, for points sampling the circle map. *Top two rows*: no noise. *Bottom two rows*: 2-dimensional Gaussian noise with standard deviation $\sigma = 0.1$ in both directions

than the $\check{D}\check{C}$ -method. To support our claim, we compute the eigenspace diagrams using the $\check{D}\check{C}$ -method with increased noise, and indeed find no false positives; see Figure 6.

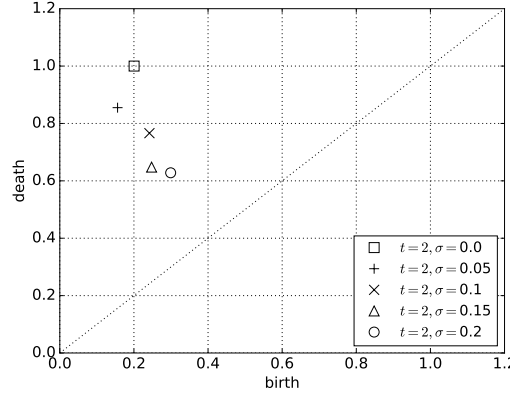


Figure 6: The superimposed eigenspace diagrams computed with the $\check{D}\check{C}$ -method of the expanding circle map for randomly chosen sets of 200 points each with isotropic Gaussian noise with increasing width σ . In each run, the only non-empty eigenspace diagram is for $t = 2$, and this diagram contains exactly one point

Torus maps. The situation is similar for the three torus maps, whose eigenspace diagrams are shown in the next three panels of Figure 5. The eigenvectors of f_1, f_2, f_3 are represented by points on the upper edges of the panels, indicating that their corresponding homology classes last until the last complex in the filtration. This is different in the VR-method because the Vietoris–Rips complex for large radii is less predictable than the Delaunay–Čech complex. In contrast to the circle map, we observe false positives also in the $\check{D}\check{C}$ -method. They show up as points with small to moderate persistence in the three diagrams. We also have false positives in the VR-method, but the results are difficult to compare because for complexity reasons we could not run the algorithm beyond $N = 200$ points. As another indication of improved accuracy of the $\check{D}\check{C}$ -method, we note that the eigenspace diagrams we observe in our experiments do not suffer the problem of abundant eigenvalues discussed in [EJM15, Section 6.4].

5.4. Runtime Analysis. We analyze the running time of the $\check{D}\check{C}$ -method for sets of N points, with N varying from 100 to 10000. For the persistent homology computation, we use coefficients in the field \mathbb{Z}_{1009} . The time is measured on a notebook class computer with 2.6GHz Intel Core i7-6600U processor and 16GB RAM.

Overall running time. We begin with a brief comparison of the two methods, first of the overall running time for computing eigenspace diagrams; see Table 2. As mentioned earlier, the VR-method uses Vietoris–Rips complexes, which grow fast with the number of points and the radius. We could therefore run this method for $N = 100$ and 150 points only, terminating the run for $N = 200$ points after half an hour. To get a better feeling for the running time of the $\check{D}\check{C}$ -method, we

Time [sec]	$N = 100$	150	200	500	1000	1500	2000	2500
VR-method	157.41	986.60	—	—	—	—	—	—
$\check{D}\check{C}$ -method	0.07	0.12	0.21	0.92	3.66	8.36	14.53	22.35

Table 2: Time needed to compute the eigenspace diagram of the expanding circle map for N points sampled near the unit circle. For $N \geq 200$, the VR-method needs more than half an hour, at which time we terminated the process.

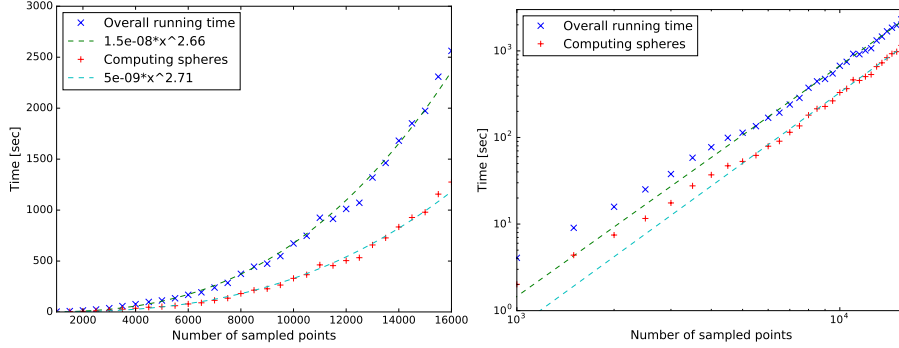


Figure 7: The time needed to compute the eigenspace diagram of the expanding circle map with the $\check{D}\check{C}$ -method as a function of the number of sampled points. We also show the amount of time spent to compute separating spheres, which is more than half the overall running time. The time for computing the Delaunay–Čech complexes and the persistence diagrams is less than 0.5 seconds in all cases and therefore not shown. To estimate the asymptotic behavior, we use the least squares technique to fit lines to the log-log data points; see the *right panel*. Excluding the results for less than $N = 5000$ points we get slopes 2.66 and 2.71, which suggests that the experimental running time of our algorithm is between quadratic and cubic in the input size.

plot the results in Figure 7, adding curves to indicate the asymptotic experimental performance. The outcome suggests that the computational complexity of the $\check{D}\check{C}$ -method is between quadratic and cubic in the number of points. We note that more than half of the time is used to compute smallest separating spheres.

Flowing an edge. To gain further insight into the time needed to flow a loop from the Čech to the Delaunay–Čech complex, we present statistics for collapsing a random edges in a variety of settings. The edges are constructed from 100, 1000, 10000 points chosen along the unit circle with added Gaussian noise, and from 100, 1000, 10000 points chosen uniformly in $[0, 1]^2$. For each data set, we pick two points at random

	Circle			Square		
	$N = 100$	1000	10000	100	1000	10000
#iterations: avg	5.27	9.09	14.70	5.47	11.98	14.60
max	9.00	13.00	19.00	9.00	16.00	17.00
#tests: avg	1.23	1.17	1.21	1.60	1.32	1.20
max	8.00	5.00	4.00	15.00	16.00	5.00

Table 3: Statistics for flowing 1000 randomly chosen edges from the Čech to the Delaunay–Čech complex. *Top two rows:* the average and maximum number of iterations of the function PHI to flow an edge from the Čech to the Delaunay–Čech complex. *Bottom two rows:* the average and maximum number of points tested inside the function GRAD to find a set for which the separating sphere does not exists.

and monitor the effort it takes to flow this edge from the Čech complex to the Delaunay–Čech complex. Specifically, we iterate the function PHI on each edge individually until the result stabilizes. The statistics in Table 3 shows how many times PHI is iterated and how many points are tested inside each call to the function GRAD. The statistics for the circle and the square are similar, with consistently larger numbers when we pick the edges in the square.

Smallest separating spheres. Our analysis shows that the DČ-method spends most of the time to compute smallest separating spheres. For this reason, we compare the straightforward implementation (function SEPARATE), with the heuristic improvement (function MOVETOFRONT). We generate the points in $[0, 1]^2$ as described above. For both functions, we randomly pick 10000 simplices from the Čech complex and test for each simplex whether or not there exists a sphere that separates the simplex from the rest of the points. Figure 8 shows that the running time of both functions depends linearly on the number of points, which is to be expected. The best-fit linear functions suggest that the move-to-front heuristic is faster than the more naive extension of the miniball algorithm to finding smallest separating spheres. The difference is more pronounced for edges of the Čech complex (left panel) for which we expect more points inside the circumscribed spheres and an early contradiction to the existence of a separating sphere. In contrast, every edge of the Delaunay–Čech complex has a separating sphere by definition.

6. DISCUSSION

The main contribution of this paper is the improvement of the algorithm for computing the persistence of a sampled self-map in [EJM15] by an order of magnitude. Substituting Delaunay–Čech for Vietoris–Rips complexes, we gain efficiency through the economy of these complexes, but we have to tackle a number of technical challenges, as described in this paper. The reported research raises a number of questions, and we list two of the more important ones here.

- Can we give theoretical upper bounds on the number of single-edge collapses needed to flow a loop from a Čech to a Delaunay–Čech complex?

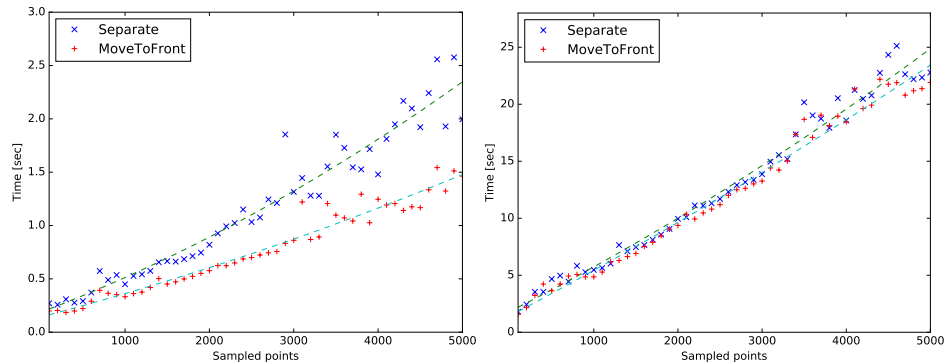


Figure 8: *Left*: the time needed to compute 10000 smallest separating spheres for randomly chosen edges from the Čech complex constructed on points sampled uniformly from $[0, 1]^2$. *Right*: the time needed to compute 10000 smallest separating spheres for edges of the Delaunay–Čech complex constructed on points sampled uniformly from $[0, 1]^2$.

- Can the computation of smallest separating spheres be improved by customizing the procedure to small sets inside the sphere, or by taking advantage of the coherence between successive calls?

REFERENCES

- [BaEd17] U. BAUER AND H. EDELSBRUNNER. The Morse theory of Čech and Delaunay complexes. *Trans. Amer. Math. Soc.* **369** (2017), 3741–3762.
- [ChOu08] F. CHAZAL AND S. Y. OUDOT. Towards persistence-based reconstruction in Euclidean spaces. In *Proceedings of the 24th ACM Symposium on Computational Geometry*, 232–241, 2008.
- [CGAL16] CGAL EDITORIAL BOARD. *CGAL User and Reference Manual*. 2016.
- [EdHa10] H. EDELSBRUNNER AND J.L. HARER. *Computational Topology. An Introduction*. Amer. Math. Soc., Providence, Rhode Island, 2010.
- [EJM15] H. EDELSBRUNNER, G. JABŁOŃSKI AND M. MROZEK. The persistent homology of a self-map. *Found. Comput. Math.* **15** (2015), 1213–1244.
- [ELZ02] H. EDELSBRUNNER, D. LETSCHER AND A. ZOMORODIAN. Topological persistence and simplification. *Discrete Comput. Geom.* **28** (2002), 511–533.
- [EdMu90] H. EDELSBRUNNER AND E.P. MÜCKE. Simulation of simplicity: a technique to cope with degenerate cases in geometric algorithms. *ACM Trans. Graphics* **9** (1990), 66–104.
- [For98] R. FORMAN. Morse theory for cell complexes. *Adv. Math.* **134** (1998), 90–145.
- [Gar99] B. GÄRTNER. Fast and robust smallest enclosing balls. In “Proc. 7th Ann. European Sympos. Algorithms, 1999”, 325–338.
- [Gro87] M. GROMOV. Monotonicity of the volume of intersections of balls. In *Geometrical Aspects of Functional Analysis*, J. Lindenstrauss and V.D. Milman (eds.), LNM **1267** (1987), 1–4.
- [KMM04] T. KACZYŃSKI, K. MISCHAIKOW AND M. MROZEK. *Computational Homology*. Applied Mathematical Sciences **157**, Springer-Verlag, New York, 2004.
- [Kir34] M.D. KIRSZBRAUN. Über die zusammenziehenden und Lipschitzsche Transformationen. *Fund. Math.* **22** (1934), 77–108.
- [WeWi75] J.H. WELLS AND L.R. WILLIAMS. *Embeddings and Extensions in Analysis*. Ergebnisse der Mathematik und ihrer Grenzgebiete **84**, Springer-Verlag, Berlin, Germany, 1975.
- [Wel91] E. WELZL. Smallest enclosing disks (balls and ellipsoids). In *New Results and New Trends in Computer Science*, H.A. Maurer (ed.), LNCS **555** Springer, (1991), 359–370.
- [Zie95] G.M. ZIEGLER. *Lectures on Polytopes*. Graduate Texts in Mathematics **152**, Springer, Berlin, Germany, 1995.